Impact of Freeze-thaw Cycles on Coatings Applied to the Surface of Alkali-activated Materials

Lukáš Procházka[1)], Adéla Brázdová[2*)]

[1)] Technical University of Ostrava, Faculty of Civil Engineering, Department of Building Materials and Diagnostics of Structures, 708 00 17. listopadu 2172/15, Czech Republic, e-mail: lukas.prochazka@vsb.cz; ORCID: https://orcid.org/0000-0002-2829-5643
[2*)] Technical University of Ostrava, Faculty of Civil Engineering, Department of Building Materials and Diagnostics of Structures, 708 00 17. listopadu 2172/15, Czech Republic, e-mail: adela.brazdova@vsb.cz; ORCID: https://orcid.org/0000-0003-1818-0540

http://doi.org/10.29227/IM-2024-02-05

Submission date: *03.06.2024.* | Review date: *19.07.2024*

Abstract

This paper focuses on the possibility of applying selected types of coatings (synthetic and epoxy) on the surface of alkali-activated materials based on finely ground granulated blast furnace slag with an admixture of cement by-pass dust and silica fly ash. Admixtures represent 30% of the binder component (15% fly ash, 15% cement by-pass dust). The mixture is activated with anhydrous disodium metasilicate. The samples were categorized into two series samples stored in water and samples wrapped in foil. Following this, the surface of these two series was modified by two methods, namely brushing with a steel brush and roughening with a diamond wheel. The properties related to the adhesion of the coating to the surface were mainly investigated before and after 100 freeze-thaw cycles. The cross-cut method and pull-off test for adhesion determined the adhesion. The cross-cut test found that the synthetic coating was less susceptible to surface modification than the epoxy coating. The samples were exposed to 100 freeze-thaw cycles. Then, the cross-cut method was applied to the coated roughened surface and the results of this test were classified into category 3. During the determination of the adhesion of the coatings by the pull-off test on the roughened surface for both methods of sample storage, the character of breakage for the synthetic coating was of the cohesive type, thus it was the tensile strength of the materials, while for the epoxy coating, it was the adhesive breakage, thus it was the adhesion between the surface and the coating.

Keywords: *Alkali-activated meterials, coating, surface modification, cross-cut test, pull-off test*

1. Introduction

Currently, the trend towards becoming carbon neutral in all respects makes it necessary to look for new technological solutions. In the construction industry, one of these solutions is the possibility of replacing clinker, which is then used to make cement. Alkali-activated concrete (AAC), which is generally considered as an alternative to traditional Portland cement-based binders [1,2], could contribute to this goal. For alkali-activated materials, it is possible to use secondary products produced when coal is burned or when iron is produced in a blast furnace. They are therefore a by-product of production and are considered secondary raw materials - for this paper, they are mainly blast furnace slag (BFS), fly ash after denitrification (FAD) or cement bypass dust (CBPD) [3-5].

Granulated Blast Furnace Slag (BFS) is an amorphous material formed during the production of iron in a blast furnace by rapid cooling of molten slag [6,7]. According to a review by Sajid, M. et al. (2019), BFS is mainly composed of oxides, namely SiO_2, CaO, $Al2O_3$, MgO, TiO_2, etc. and impurities like FeO, MnO, P_2O_5, and S [6].

Fly ash (FA) is generated from the combustion of coal. Fly ash from coal combustion contains mainly SiO_2, Al_2O_3, Fe_2O_3 and, depending on the combustion technology, varying amounts of CaO [8]. Coal combustion releases nitrogen oxides into the air, which must be reduced, e.g. by Selective catalytic reduction (SCR) and selective non-catalytic reduction (SNCR) [5]. Concrete using FA shows improved plasticity, decreased adiabatic temperature rise; reduced permeability, and reduced possibility of alkali-silica reaction and sulphate attack [9]. However, the authors Michalik, A. et al. (2019) also state that denitrification can lead to the deterioration of fly ash properties and thus deterioration of cement (concrete) properties. For our paper, it was fly ash after denitrification (FAD) was used.

According to a study by Taha, R. et al. (2002), the composition of CBPD is more than 60% CaO and other significantly represented components are SiO_2, Al_2O_3, Fe_2O_3, K_2O, Na_2O, Cl^-, etc. [10]. However, according to a study by Wojtacha-Rychter, K. (2022), the compressive and flexural strength of concretes with CBPD decreases with the amount of this material used [11].

This paper aims to prepare test samples made from secondary raw materials. For this purpose, admixtures were created with a total of 30% binder component (15% FAD, 15% CBPD) and BFS (70%). The samples will be subsequently surface coated. Additionally, the adhesion of the coatings to the surface will be tested.

2. Materials and Methods

In the experiment, secondary raw materials were activated with anhydrous disodium metasilicate (ADM). The following raw materials were used: fly ash after denitrification (FAD) from the Ostrava Třebovice power plant, cement by-pass dust (CBPD) from the Cemmac Horné Srnie cement plant and finely ground granulated blast furnace slag (BFS). While BFS and siliceous FAD are commonly used in cement and concrete practice, the usage of CBPD is limited by its chemical composition and its variability, especially the high content of chlorides (6.7 wt.%), sulphates, alkali and free lime. The sand of 0/4 mm fraction from the Tovačov locality was used as an aggregate. The chemical composition of the input materials was determined by XRF analysis and is given in Table 1, the physical properties (particle size, specific gravity and specific surface area) are shown in Table 2 and the ADM properties are presented in Table 3.

Tab. 1. Content of selected oxides in input raw materials. (LOI—loss on ignition).

Oxide	Content [%]		
	FAD	CBPD	BFS
SiO_2	50.89	4.90	33.81
Al_2O_3	21.34	1.49	8.14
Fe_2O_3	9.49	1.77	0.32
CaO	4.48	41.54	46.16
SO_3	0.58	1.73	1.46
K_2O	3.14	14.22	0.42
MgO	1.67	0.37	7.86
LOI	6.27	25.87	-0.09

Tab. 2. Selected physical properties of input raw materials.

	Q10 [µm]	Q50 [µm]	Q90 [µm]	Surface area [m^2/kg]	Specific density [kg/m^3]
CBPD	1.27	4.36	36.50	~ 520	2 610
FAD	1.87	9.56	33.08	~ 500	2 240
BFS	2.32	11.92	32.67	≥ 400	2 860

Tab. 3. Composition of anhydrous disodium metasilicate [12].

ADM	Unit	Value
SiO_2 content	%	min. 44
pH	-	12.5
molar weight	kg/mol	122.06
relative density	g/cm^3	2.6

The mixture called REC 3 was used in this experiment and has already been extensively tested and published in previous research, but this paper brings new insights [13-15]. This mixture was selected for further testing due to performing comparable or better results than the other previously tested hybrid alkali-activated mixtures. Besides the physical properties, another major advantage (compared to the other mixes tested) is that this mixture contains a small amount of activator, which is considered to impact the overall costs positively. The same mixture (REC 3) was used for this paper, with only one modification - compared to the previous research, an ordinary sand of 0/4 mm fraction was used (in the last research, a standard quartz sand of 0/2 mm fraction was used). Therefore, the main binder component in this mixture is BFS (70% of the total binder component) and the admixtures FAD and CBPD (equally 15% of the binder component). Complete mixture composition for preparation of one standard form for 3 prism samples (40x40x160) mm is given in Table 4.

Tab. 4. Complete mixture components preparing of one standard form 3x (40x40x160) mm.

Materials [g]	BFS	FAD	CBPD	ADM	W	Sand
REC 3	315	67.5	67.5	62.30	215	1350

Prisms (40x40x160 mm) and tiles (300x300x40 mm) were prepared for the experiment. To simulate the smooth surface of concrete structures (system formwork), plastic forms greased with coconut emulsion were used to prepare the tiles - f.e. in producing concrete elements by the vibro-pressing compaction process, the surface of the concrete product is rougher due to the designed mix and production method. Subsequently, the samples were divided into two series after 2 days of demoulding. One group was stored for maturation as standard (labelled 'W') and the second was wrapped in foil. The surfaces of the test bodies were prepared in two ways: the prisms and part of the tiles were roughened with a steel brush (labelled ‘B’) and the remaining tiles were roughened with a diamond grinding wheel (labelled ‘R’). Subsequently, all samples were cleaned of dust using compressed air and vacuumed.

Before the application of the coating, the moisture content of the materials was determined gravimetrically on selected prisms (according to ISO 12 570) [16] - the formula for calculating the moisture content is given in Equation 1, where ‘m’ means the weight of the sample before drying [kg] and ‘m0’ means the weight of the dried sample [kg]. the result is then given in mass %. The remaining samples' moisture content was also verified by material moisture meter GMK 100 (Greisinger electronic, Senseca Germany GmbH, Germany) [16].

$$u = \frac{m - m_0}{m_0} \tag{1}$$

Subsequently, the samples were left in a laboratory environment to dry to a stable weight before applying the coating. This experiment used two types of coatings, namely, two-component water-soluble epoxy coating (E) (producer MC-Bauchemie) and synthetic coating (S) (producer Datecha). The coatings were carried out according to the requirements specified by the producers and applied by roller - the first coating served as a primer (penetration) and the second was the final. Before the next testing was verified dry film thickness (according to EN ISO 2808 method 10) [17] with an ultrasonic thickness gauge - PosiTector 200 (producer Berg Engineering & Sales, Company, Inc., Rolling Meadows, IL, USA). According to EN 1542 [18] was determined the reference tensile (cohesion/adhesion) strength of the tested material by the R-mixture (Proceq DY-216; Screening Eagle Technologies AG, Switzerland). Coating adhesion to the surface was performed according to the same procedure on both surface modifications (R, B).

The adhesion of the coating to the surface was also evaluated using the cross-cut method according to ČSN EN ISO 2409. This

test was carried out on a third type of surface, namely the surface without modification (WM), the surface was only cleaned of dust. The principle of this method is to cut through the coating with a rectangular grid penetrating to the surface, detecting the characteristics that are determined by the adhesion of the coating to the surface. The measured and determined quantities are not defined in this case. The classification was carried out using a Keyence optical digital microscope, where the test surface was scanned and the software was used to calculate the tear-off area, followed by the percentage of damage.

For this article reference strengths were samples placed in a stable climate humidity chamber with a temperature of 20 ± 2°C and a relative humidity of 98% for 28 days. Subsequently were determined compressive and flexural strengths (Form+Test MEGA 100-300-10 DM1 hydraulic press with Proteus software) according to the EN 196-1 standard. The uniform loading speed was set for flexural strength (50 ± 10) N/s and for compressive strength (2400 ± 200) N/s [19].

Simultaneously was for the determination of frost resistance occurred in a freezer with automatic cycling (according to ČSN 72 2452) - cycling temperatures were in the range of −15 to −20 °C for freezing and a water bath for thawing with a temperature of 20 °C (one cycle consists of 4 hours of freezing and 2 hours of thawing) [20]. After the freeze-thaw test, the cross-cut method and the pull-off test were applied again. The samples tested after the freeze-thaw test are marked (F). The procedure of all the performed tests is shown in FIGURE 1.

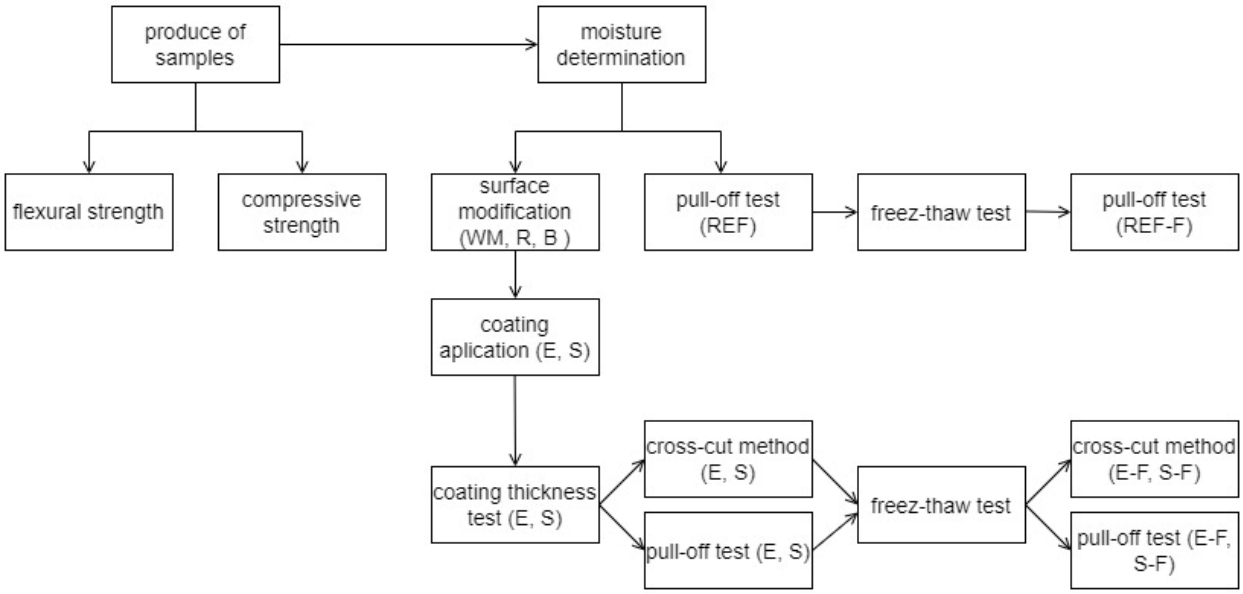

Fig. 1. Experiment flow chart.

3. Results

For this article, the 28-day compressive and flexural strengths were tested only (this mixture had been examined in previous studies). The compressive strength was around 68 MPa and the flexural strength was around 6.5 MPa. These results are slightly lower than when using standard quartz sand, where the results were published in [13,15], but the differences were only within standard deviations.

According to the manufacturer's guidelines, the synthetic coating (S) can be applied only to surfaces with a moisture content lower than 15% - the moisture content of the samples had been determined before sample preparation and coating application. On the other hand, there is no strictly defined maximum moisture content for the two-component epoxy coating (E) but the coating must not be applied to a surface with distinct moisture maps. Moisture content has been determined by two methods - gravimetrically and by a material moisture meter. The gravimetric method stated the moisture content of samples to 7.2% for REC 3 samples and 7.4% for REC 3 W samples. The material moisture meter stated a moisture content of about 6.7% for both storage methods. This test confirmed the manufacturer's requirements for minimum coating thickness. The dry film thickness determination results using the ultrasonic thickness gauge are shown in Table 5. Data with thickness are available on an open repository [21].

Tab. 5. The text of the table caption will be here.

	REC 3						REC 3 W					
Surface modification	**WM**		**B**		**R**		**WM**		**B**		**R**	
Coating type	**E**	**S**	**E**	**S**	**E**	**S**	**E**	**S**	**E**	**S**	**E**	**S**
Thickness [µm]	112.7	173.6	109.6	170.9	136.5	194.7	111.1	171.8	110.0	170.9	119.5	187.8
Standard deviation [µm]	7.52	8.78	7.39	6.12	6.47	5.17	8.26	8.73	4.78	13.33	7.86	3.17
Min. [µm]	99	164	101	162	127	184	102	159	103	150	110	182
Max. [µm]	126	190	128	181	147	203	130	188	117	194	134	195
Median [µm]	110	171	107.5	169.5	137	194	112	169	109	171.5	117	188
Modus [µm]	108	164	105	181	128	190	106		107		115	188

It is evident from Table 5 that there is only a minimal difference in dry film thickness between the surface without modification and the surface modified with the steel brush for both types of coating, with slightly higher thicknesses achieved for the surface without modification. Higher dry film thicknesses were obtained for the diamond wheel's roughened surface, which may be related to the roughness of the surface, where a slightly higher amount of paint needs to be applied for a rougher surface, which correlates

with the resulting dry film thickness. Between the comparisons of the different types of paint, a higher dry film thickness was observed for the synthetic paint in all cases.

Based on the thickness of the dry film result, the distance between each cut was determined for the cross-cut test. The distance was taken based on the average value of a series of measurements. For film thicknesses from 61 to 120 µm, the cut spacing is 2 mm, and this spacing was used for almost all epoxy-coated series except for the REC 3-R set, where a cut spacing of 3 mm was used due to the 136 µm thickness. For dry film thicknesses from 121 to 250 µm, a 3 mm cutting distance is given, which was used for all series with synthetic coating. The results of the evaluation of the grid method are shown in Table 6. The damaged area of the coating was determined and calculated by Keyence optical digital microscope (shown in FIGURE 2.) - by the axis of the edge sections, then the damaged areas were selected using the software and the damaged area in % was calculated.

Tab. 6. Results and evaluation of coating adhesion determined by the cross-cut method (X - the sample was not tested).

	REC 3		**REC 3 W**	
	Damage [%]	**Classification class**	**Damage [%]**	**Classification class**
E-WM	53.22	4	100.00	5
S-WM	24.62	3	20.35	3
E-R	4.94	1	4.63	1
S-R	3.57	1	8.15	2
E-B	76.26	5	92.30	5
S-B	16.63	3	20.74	3
E-R(F)	17.35	3	32.90	3
S-R(F)	16.97	3	19.64	3
E-B(F)	83.62	5	X	X
S-B(F)	32.87	3	56.27	4

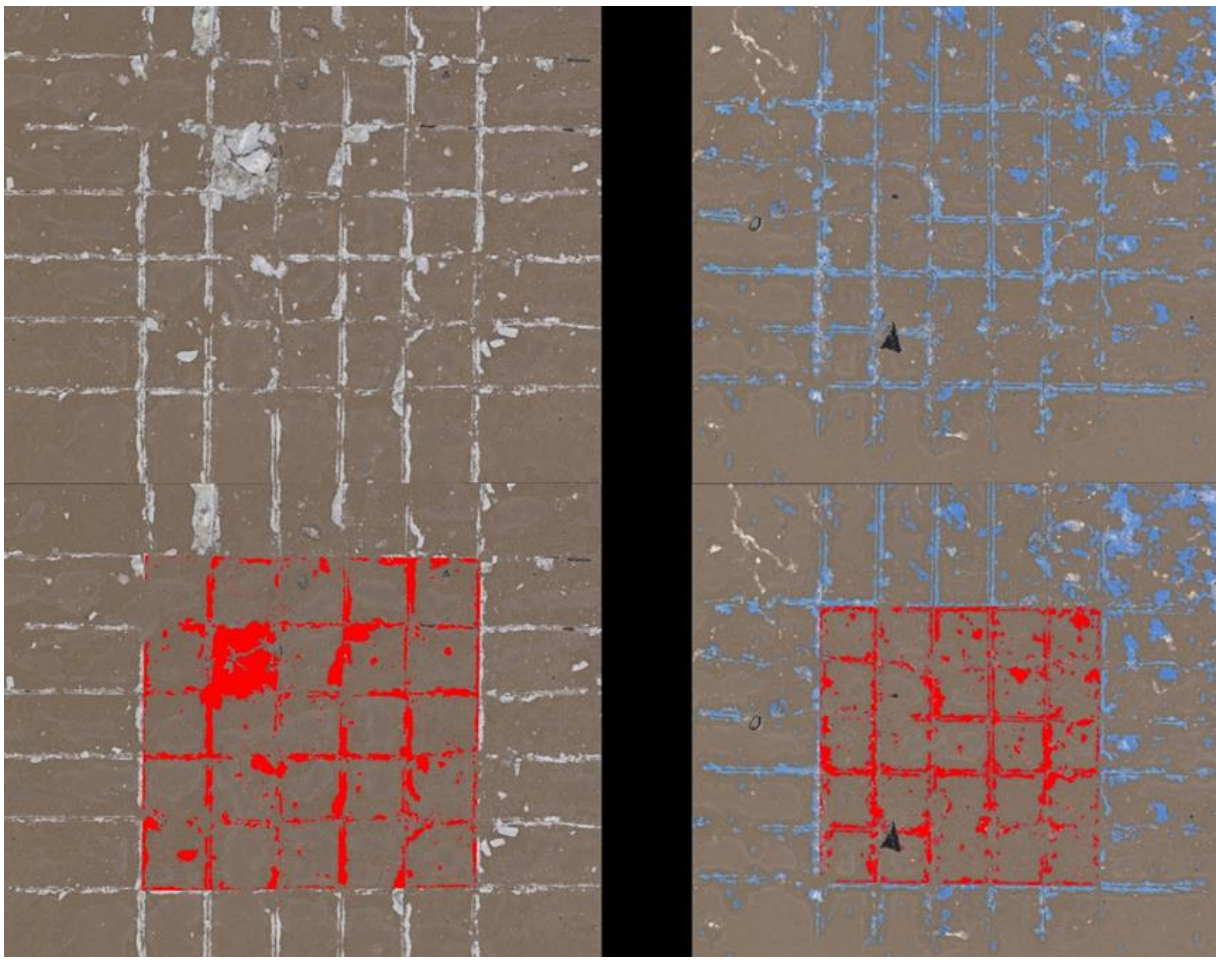

(a) (b)

Fig. 2. Example of the evaluation of the cross-cut method using microscopy and image analysis – (a) example cross-cut method on epoxy coating, (b) example cross-cut method on synthetic coating

The results of the adhesion of the coatings to the surface determined by the cross-cut method show that the epoxy coating used is characterized by a higher sensitivity to surface modification before the coating is applied. If the surface is sufficiently roughened before coating, both types of coatings are characterised by good adhesion to the surface. However, if the surface is not modified or only slightly modified, the synthetic coating is characterised by a higher adhesion than the epoxy coating. This may be caused by the fact that the synthetic coating is more diluted for the penetration layer, so it penetrates deeper into the surface and consequently

the coating is characterized by better adhesion. All observed samples and coatings demonstrated a deterioration in adhesion properties after 100 freeze-thaw cycles. The synthetic coating was characterized by a level of damage below 20% for the roughened samples in the cross-cut method. If we take the same evaluation as for strengths, where the strength drops must not exceed 25%, it can be said that with this combination (between material, coating and preparation) the adhesion of the coating to the surface can be considered as frost resistant.

Pull-off tests were also performed to determine the adhesion of the coating to the surface and to determine the tensile strength (cohesion) both before and after 100 freeze-thaw cycles. The results of the pull-off tests are shown in FIGURE 3.

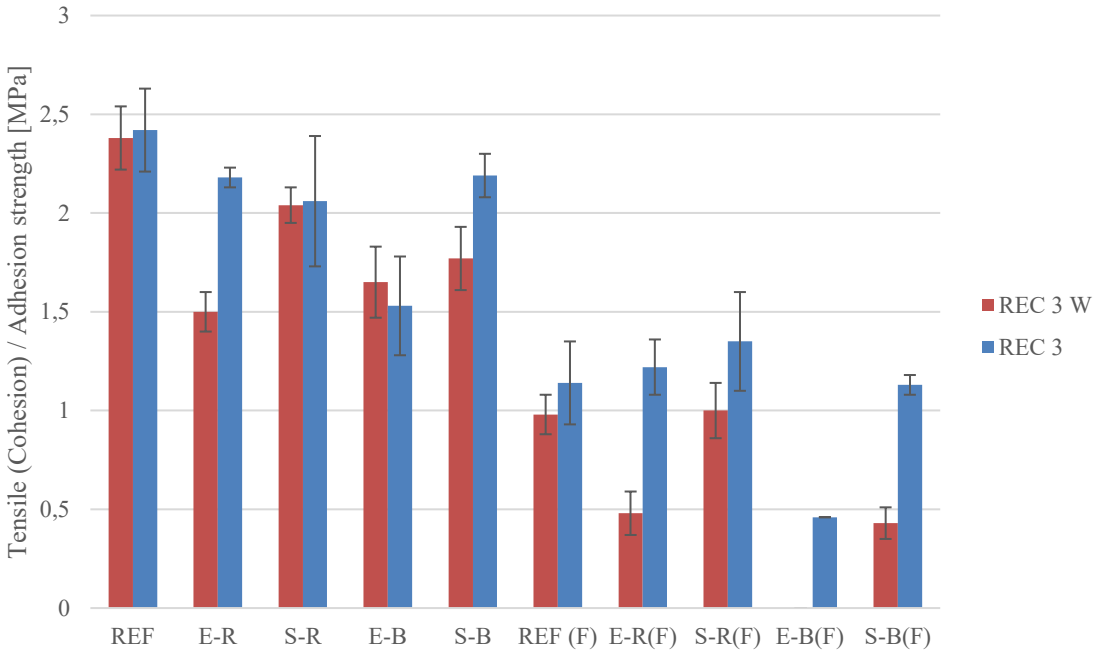

Fig. 3. Comparison of pull-off test results.

The minimum tensile strength of the synthetic coating given by the manufacturer is 1.5 MPa, therefore a pull-off test was carried out before the application of the coating to determine if the coating could be applied. The tensile strength for both series (REC 3 and REC 3 W) was around 2.4 MPa, so the coating could be applied. The samples stored in the foil have a higher tensile strength (coating adhesion) than samples stored in water, which is also valid for the case before and after 100 freeze-thaw cycles. The highest pull-off resistance values were achieved for the samples E-R, S-R and S-B in REC 3 series. The lowest cohesive strength was obtained for the sample E-R for the REC 3 W series. After 100 freeze-thaw cycles were significant decreases in the cohesion and adhesion strength values. In the REC 3 series, strength drops ranged from 35 to 50% for the samples S-R(F), E-R(F), S-B(F) and around 70% for the sample E-B(F) - there was only one test spot due to coating damage after the freeze-thaw process. For the brushed surface of the REC 3 W series, the drops ranged from 50 to 70% and for the sample S-B(F) the strength drop was 75%. Sample E-B(F) was not tested due to extensive paint damage. In terms of the type of failure after 100 freeze-thaw cycles, the synthetic coating was cohesive failure (tensile strength of the material) while the epoxy coating was predominantly adhesive failure, i.e. the adhesion of the coating to the surface. The frost resistance coefficient of tensile strength for the REC 3 series is 0.47 and for the REC 3 W series is 0.41, so this material cannot be considered frost resistant in terms of tensile strength. Although the frost resistance coefficient for compressive strength and flexural strength was around 1 [13].

4. Discussion

In addition to traditional coatings such as acrylic, epoxy, polyurethane, or polymer emulsions [22], it is also possible to use less traditional coating systems based on alkaline activated materials (AAM) [23]. For AAM-based coatings, it is necessary to limit shrinkage during hydration and to ensure sufficient interactions with the surface. The shrinkage of these coatings is determined by the type of input raw materials, the curing temperature, the silicate module of the used activator and the amount of alkali used for the alkali activation [23]. It is generally considered that the highest shrinkage is achieved in alkali-activated BFS, and this can be reduced by using mineral admixtures such as fly ash, metakaolin or silica fume [24-27]. For coating AAMs, it is also important to which material they are applied. When applied to a stainless steel or aluminium surface, aluminium can cause negative corrosion leading to low adhesion strength. For stainless steel, Cr can inhibit the curing reaction, leading again to the formation of a weak adhesive strength. For example, when a metakaolin-based coating was applied to a glass surface, no chemical reaction between the coating and the surface was observed. On the other hand, when an AAM coating was applied to a concrete surface, a chemical reaction between the concrete substrate and the AAM coating was observed. When the coating is applied, the CSH gels disintegrate, followed by reaction with an alkali activator, leading to the formation of CSH gel. This makes the layer between the AAM coating and the concrete surface more uniform and makes the interface characterized by a stronger bond [23].

5. Conclusion

The determination of adhesion by the cross-cut method shows that the epoxy coating is much more sensitive to surface modification than the synthetic coating. The tested mixture cannot be considered to be frost resistant in terms of tensile strength, and the applied coatings cannot be considered to be frost resistant in this combination. From the failure behaviour after 100 freeze-

thaw cycles, it can be concluded that the adhesion of the synthetic coating is sufficient since cohesive failure occurred during the pull-off test. On the other hand, the adhesion of the epoxy coating to the surface is less than the tensile strength of the material, because, after 100 freeze-thaw cycles, adhesion failure occurred during the pull-off test.

Acknowledgments

This paper was created as part of the project No. CZ.02.01.01/00/22_008/0004631 Materials and technologies for sustainable development within the Jan Amos Komensky Operational Program financed by the European Union and from the state budget of the Czech Republic. The authors thank the Department of Thermal Engineering from VSB-Technical University of Ostrava for performing XRF analyses.

References

1. B. C. Mendes, L. G. Pedroti, C. M. F. Vieira, M. Marvila, A. R. G. Azevedo, J. M. Franco de Carvalho and J. C. L. Ribeiro, "Application of eco-friendly alternative activators in alkali-activated materials: A review". Journal of Building Engineering 35, 102010 (2021).
2. V. Bílek, J. Hurta, P. Done and L. Žídek, "Development of alkali-activated concrete for structures – Mechanical properties and durability", Perspectives in Science 7, 190-194 (2016).
3. T. Luukkonen, Z. Abdollahnejad, J. Yliniemi, P. Kinnunen and M. Illikainen, "One-part alkali-activated materials: A review", Cement and Concrete Research 103, 21-34 (2018).
4. B. Vojvodíková, L. Procházka and J. Boháčová, "X-ray Diffraction of Alkali-Activated Materials with Cement By-Pass Dust", Crystals 11(7), 782 (2021).
5. A. Michalik, J. Babińska, F. Chyliński and A. Piekarczuk, "Ammonia in Fly Ashes from Flue Gas Denitrification Process and its Impact on the Properties of Cement Composites", Buildings 9(11), 225 (2019).
6. M. Sajid, C. Bai, M. Aamir, Z. You, Z. Yan, & X. Lv, "Understanding the Structure and Structural Effects on the Properties of Blast Furnace Slag (BFS)", ISIJ International 59(7), 1153–1166 (2019).
7. Y. Kang, C. Liu, Y. Zhang, H. Xing and M. Jiang, "Crystallization behavior of amorphous slag beads prepared by gas quenching of blast furnace slag", Journal of Non-Crystalline Solids 500, 453–459 (2018).
8. Z. Giergiczny, "Fly ash and slag", Cement and Concrete Research 124, 105826 (2019).
9. L. Pazdera, L. Topolar, M. Korenska, J. Smutny and V. Bilek, "Advanced Analysis of Acoustic Emission Parameters during the Concrete Hardening for Long Time," in 11th European Conference on Non-Destructive Testing (ECNDT 2014), October 6-10, 2014, Prague, Czech Republic.
10. R. Taha, A. Al-Rawas, A. Al-Harthy and A. Qatan, "Use of Cement Bypass Dust as Filler in Asphalt Concrete Mixtures", Journal of Materials in Civil Engineering 14(4), 338-343 (2002).
11. K. Wojtacha-Rychter, M. Król, M. Gołaszewska, J. Całus-Moszko, M. Magdziarczyk and A. Smoliński, "Dust from chlorine bypass installation as cementitious materials replacement in concrete making", Journal of Building Engineering 51, 104309 (2022).
12. Penta Chemical Unlinited–Chemikalie. Available online: https://www.pentachemicals.eu/chemikalie (accessed on 12 January 2024).
13. L. Procházka, J. Boháčová and B. Vojvodíková, "Effect of Admixtures on Durability and Physical-Mechanical Properties of Alkali-Activated Materials" Materials 15(6), 2010, (2022).
14. L. Procházka, B. Vojvodíková and J. Boháčová, "Possibilities of Application Cement By-Pass Dust into the Garden Architecture Elements", Crystals 11(9), 1033 (2021).
15. L. Procházka, A. Brázdová, "Surface modification of alkali-activated materials with regard to durability", in 16th International Scientific Conference of Civil and Environmental Engineering for PhD Students and Young Scientists, (proceedings 2024), in press.
16. ČSN EN ISO 12570 (730573) Hygrothermal performance of building materials and products - Determination of moisture content by drying at elevated temperature.
17. EN ISO 2808 Paints and varnishes – Determination of film thickness; Office for Technical Standardization, Metrology and State Testing: Prague, Czech Republic (2020).
18. EN 1542 Products and systems for the protection and repair of concrete structures - Test methods - Measurement of bond strength by pull-off; Office for Technical Standardization, Metrology and State Testing: Prague, Czech Republic, (2000).
19. EN 196-1 Methods of Testing Cement—Part 1: Determination of Strength; Office for Technical Standardization, Metrology and State Testing: Prague, Czech Republic, (2005; pp. 5–40.).
20. CSN 722452 Frost Resistance Test of Mortar; Office for Technical Standardization, Metrology and State Testing: Prague, Czech Republic, 1970; Classifier 722452.
21. Open repository on ZENODO. https://doi.org/ 10.5281/zenodo.11453028

22. A. A. Almusallam, F. M. Khan, S. U. Dulaijan and O. S. B. Al-Amoudi, “Effectiveness of surface coatings in improving concrete durability”, Cement and Concrete Composites 25(4–5), 473–481 (2003).
23. Q. Tian, S. Wang, Y. Sui and Z. Lv, “Alkali-activated materials as coatings deposited on various substrates: A review”, International Journal of Adhesion and Adhesives 110, 102934 (2021).
24. S. Aydın, “A ternary optimisation of mineral additives of alkali activated cement mortars”, Construction and Building Materials 43, 131–138 (2013).
25. Z. Li, T. Lu, X. Liang, H. Dong and G. Ye, “Mechanisms of autogenous shrinkage of alkali-activated slag and fly ash pastes”, Cement and Concrete Research 135, 106107 (2020).
26. Y. Ma, X. Yang, J. Hu, Z. Zhang and H. Wang, “Accurate determination of the “time-zero” of autogenous shrinkage in alkali-activated fly ash/slag system”, Composites Part B: Engineering 177, 107367 (2019).
27. Z. Li, M. Nedeljkoviü, B. Chen, & G. Ye, “Mitigating the autogenous shrinkage of alkali-activated slag by metakaolin”, Cement and Concrete Research 122, 30–41 (2019).